
PEPICO ANALYSIS OF CATALYTIC REACTOR EFFLUENTS AT THE FINESTBEAMS BEAMLINE OF MAX IV LABORATORY: DME CONVERSION OVER A ZSM-5 ZEOLITE

A PREPRINT

Morsal Babayan*

Nano and Molecular Systems Research Unit
University of Oulu
Oulu, Finland
morsal.babayan@oulu.fi

Evgeniy Redekop

Department of Chemistry
Centre for Materials Science and Nanotechnology (SMN)
University of Oslo
Oslo, Norway
evgeniy.redekop@smn.uio.no

Esko Kokkonen

MAX IV Laboratory
Lund University
Lund, Sweden

Unni Olsbye

Department of Chemistry
Centre for Materials Science and Nanotechnology (SMN)
University of Oslo
Oslo, Norway

Marko Huttula

Nano and Molecular Systems Research Unit
University of Oulu
Oulu, Finland

Samuli Urpelainen*

Nano and Molecular Systems Research Unit
University of Oulu
Oulu, Finland
Samuli.Urpelainen@oulu.fi

ABSTRACT

The Methanol-To-Hydrocarbons (MTH) process involves the conversion of methanol, a C1 feedstock that can be produced from green sources, into hydrocarbons using acid zeolite or zeotype catalysts Olsbye et al. [2012]. The reaction that occurs in zeolites yields a complex mixture of multiple isomers and species, which poses challenges for effluent analysis. The conventional gas-phase chromatography (GC) method, typically employed for effluent analysis Hemberger et al. [2020], is often insufficient for separating isomers or detecting highly reactive molecules, especially with increased time resolution. As a potential solution, here, photoelectron–photoion coincidence (PEPICO) analysis of dimethyl ether (DME) flown through a zeolite catalyst (ZSM-5) has been performed at the FinEstBeAMS beamline of the MAX IV. Even-though, due to the specific configuration of the reactor packing, highly-reactive intermediates are not detected, the ratio of xylene isomers in the product stream is quantitatively determined by deconvoluting the coincidence photoelectron spectra.

Keywords PEPICO · Synchrotron radiation · Electron spectroscopy · Ion mass spectrometry · Zeolite catalyst · Isomer selectivity · Dimethyl Ether to Hydrocarbons conversion · Reactor effluent analysis

1 Introduction

Catalytic transformations of hydrocarbons and other organic molecules inside microporous acidic zeolites drive many large scale industrial chemical processes with enormous combined economic and environmental impact. Some of zeolite-mediated catalytic processes are also key candidates for implementing more sustainable transformations of diversified raw materials and renewable energy into vital energy carriers and chemical intermediates. Highly convoluted reaction networks and microporous transport phenomena involved in catalysis by zeolites often present formidable

experimental challenges. Complex effluent streams produced by zeolite catalysts may contain dozens of compounds, many of them present in several isomeric forms. Gas chromatography (GC) is a commonly used technique for effluent analysis in laboratory experiments that are typically conducted at ambient or above-ambient pressure conditions. However, GC is limited in time resolution and its ability to capture highly reactive closed and open shell gaseous intermediates, e.g. formaldehyde, ketenes, or radicals. Kinetic measurements under well-defined, low pressure reaction conditions have emerged as an important source of mechanistic information because these highly reactive intermediates can be more readily detected and quantified by mass-spectrometry. Likewise, low pressure operation prolongs the catalyst lifetime by minimizing secondary reactions and coking, thus expanding the range of catalyst states that are amenable for precise kinetic characterization Redekop et al. [2020].

Photoionization Mass-Spectrometry (PIMS) provides a suitable analytical platform for advanced mechanistic investigations, whereby an analyte is ionized by an incident photon and the resulting photoions are detected. PIMS achieves its full analytical potential when energy of the incident light can be varied in the Vacuum Ultraviolet (VUV) range (6–42 [eV]), which typically requires a synchrotron radiation source. In comparison with conventional electron impact ionization MS and gas chromatography, PIMS-based effluent analysis offers unique analytical advantages including (i) better sensitivity and resolving power even for highly reactive species, (ii) applicability across a broad range of operating conditions, from vacuum to ambient pressure (with differential pumping), and (iii) in many cases, when performed with high photon energy resolution, can offer isomer selectivity, which is particularly valuable for organic reactions. However, in order to have a better insight into the gaseous composition, molecular photofragmentation must be considered in considerable depth Kooser et al. [2020]. Although the electron and ion spectroscopy methods alone play a major part in studying molecular photofragmentation, in particular, recording and analyzing electrons and ions originating from the same photoionization event can lead to more complete understanding of the photofragmentation process and the composition of the effluent gas stream. Taking the type of the detected particles into account, coincidence techniques may be classified as photoelectron–photoion coincidence (PEPICO), photoion–photoion coincidence (PIPICO), photo-electron–photoion–photoion coincidence (PEPIPICO), photoelectron–photoelectron coincidence and photoion–neutral coincidence Arion and Hergenhahn [2015]. PEPICO and Threshold PIMS have been most instrumental in unraveling the reaction mechanisms of Methanol-To-Hydrocarbons (MTH), catalytic pyrolysis, and oxychlorination processes. Despite the increasing interest in applying these methods to investigate catalytic reactions, few experimental setups exist which combine catalytic microreactors with PIMS-based effluent analysis.

Herein, we report the establishment of such instrument at the gas-phase end station of the FinEstBeAMS beamline of MAX IV Laboratory. As of the submission date of this article, there were only a handful of synchrotron beamlines providing capabilities for the PIMS-based analysis of catalytic reactor effluents, including FinEstBeAMS. Features of some of them are compared in Table 1. The main differences between these setups are the accessible energy ranges and the types of available detectors. While the VUV beamline at SLS offers photons in the 3–150 [eV] range and is capable of both photoion and photoelectron analysis, the BL03U beamline at NSRL has a relatively narrow photon energy range of 5–21 [eV] and only detects photoions. In comparison, FinEstBeMS covers a broad range of photon energies 4.5–1300 [eV], which enables both valence and core ionization, and features photoion and photoelectron analysis as well as coincidence experiments.

The conversion of Methanol and/or Dimethyl Ether (DME) to hydrocarbons, abbreviated MTH and DTH, respectively, on acidic zeolites and zeotypes offers a prototypical example of a catalytic reaction which produces compositionally and isomerically complex effluents. MTH/DTH are promising industrial routes towards hydrocarbon fuels and platform chemicals, which can accommodate diverse feedstocks including bio-gas and captured CO₂. In acidic zeolite or zeotype catalysts, an equilibrated mixture of DME and methanol react on Bronsted Acid Sites (BAS) to produce larger hydrocarbon molecules including alkenes, alkanes, and aromatics. The reaction proceeds through the dual-cycle Hydrocarbon Pool (HCP) mechanism in which several pathways can be distinguished. The first C–C bonds are formed from DME and/or methanol via Surface Methoxy Species (SMS) and highly reactive intermediates such as formaldehyde or ketene, eventually leading to C₂–C₃ alkenes. These primary products are then repeatedly methylated by SMS (stepwise pathway) or gaseous DME/methanol to form C₃–C₅+ alkenes – the so-called alkene cycle. The product distribution is further controlled by co-occurring cracking reactions. Hydrogen transfer reactions between methanol and alkenes, also catalyzed by BAS, lead to the formation of alkanes and aromatics. The latter can sustain an independent cycle of sequential methylation and cracking – the aromatics cycle. At steady-state, the population of *in situ* generated alkene and aromatics intermediates termed the HCP resides within the catalyst and mediates continuous catalytic production of products from DME/methanol, in parallel with the hydrogen transfer and isomerisation reactions. Moreover, methyl radicals were also detected in the reaction medium, suggesting that the underlying chemistry may be even more complex than previously thought. Eventually, the growth of large polyaromatic molecules and coke occludes the microporous space and deactivates the catalyst. Catalytic performance, i.e. activity, selectivity, and stability, is ultimately controlled by a multitude of factors related to the catalyst structure and operating conditions.

In order to establish the structure-performance relationships and optimize the catalytic materials and reactions, it is imperative to better understand the kinetics of different reaction pathways and how they are affected by variations of the materials composition and structure. However, disentangling the distinct reaction pathways and individual reaction steps is a challenging experimental task, given the aforementioned complexity. PIMS-based methodologies for the reaction analysis have already provided essential mechanistic insights into MTO chemistry, and this provides the main motivation for the current study - to showcase the new *operando* PEPICO capabilities at the FinEstBeAMS beamline in the context of this important reaction. In particular, we demonstrate PEPICO analysis of DME conversion on a ZSM-5 (MFI) catalyst with a particular emphasis on quantitative isomer discrimination for the product xylenes.

2 PEPICO

Herein, products of the DME reaction over the H-ZSM-5 zeolite catalyst are analyzed by *operando* PEPICO spectroscopy. Aside from being isomer-selective, this technique is able to qualitatively differentiate short- and long-lived species as well. With the aid of *in situ synchrotron radiation photoionization mass spectrometry*, Wen et al. [2020] have detected formaldehyde (HCHO), an active intermediate, during the MTH reaction over two various catalysts. Recently, Cesarini et al. [2022] utilized *operando* PEPICO spectroscopy to investigate reaction pathways for MTH and MCTH (methyl chloride-to-hydrocarbons) over the H-ZSM-5 zeolite catalyst. By using this technique, short-lived active intermediates, such as ketene and methyl radicals, were directly observed.

In PEPICO spectroscopy, both the photoelectron and the photoion generated via the ionization are detected. For regular PEPICO spectroscopy, the kinetic energy of electrons in conjunction with cations with same mass per charge ratio provides the mass-resolved photoelectron spectrum (ms-PES) for that specific cation. However, in threshold-PEPICO spectroscopy, photoions in coincidence with electrons having near-zero kinetic energy are collected. Therefore, mass-selected threshold photoelectron spectrum (ms-TPES) is provided for a particular mass per charge ratio by threshold-PEPICO Bodi et al. [2013]. To detect different isomers using threshold-PEPICO, tunable light sources with enough resolution, which are limited and heavily overbooked, are required. Hence, the regular PEPICO technique (from hereon PEPICO), readily available at FinEstBeAMS, is considered in this study.

The products of the reaction and the remaining reactant (when the conversion rate is less than 100%) leaving the microreactor are ionized by the photon beam. It leads to the generation of ions and electrons in the extraction region of the time-of-flight(TOF) mass spectrometer. When an electron is detected by the electron analyzer (in this study a hemispherical electron analyzer), a signal is generated to initiate a pulsed electric field in the extraction region of the mass spectrometer (a Wiley-Maclaren TOF, in this study). This field propels the cations towards the ion detector. Subsequently, the ions enter the acceleration region, where they receive additional acceleration along the axis of the spectrometer. These high kinetic energy ions fly through the drift tube with constant electric potential, consequently without experiencing any forces. Ions with different kinetic energy have different TOFs which makes it possible to distinguish them. Not only the flight times of ions in drift tube depend on their mass and velocity, i.e. their kinetic energy (similar to the electrons flight times), but their charge also affects their arrival time Wiley and McLaren [1955]. Since the electron mass is negligible comparing to the ions, the flight times of electrons are significantly lower than the ions, therefore it is reasonable to assume that the formation of the ions and the detection of the electron occur concomitantly. Eventually, the electron-ion pairs associated with the same photoionization event can be distinguished by correlating the detected electrons and ions.

2.1 True/false coincidences

Although one electron is detected each time, ionizing more than one atom or molecule throughout the ionization process is possible which leads to detect the electron/ion pairs that are not coming from the same event. Such events are known as false coincidences. By applying low ionization rate, the probability of detecting the electron/ion pairs arising from the same event (true coincidences) increase. Because the generated electron/ion pairs will be well-separated in time Bodi et al. [2013]. Furthermore, less than 100 percentage detection efficiency of the electron and ion detectors (which is lower for the electron) contributes to report the false coincidences. To distinguish the ions generated by true coincidences, subtracting the random ions coming from the false coincidences is required. Consequently, a reference random coincidence must be measured under exactly the same conditions. Hence, an external pulse generator is used to create artificial random triggers besides electron triggers. For those random triggers, all measured coincidences would be false coincidences. Eventually, subtracting the random coincidences from total coincidences arisen from electron triggers, leads to true coincidences. Prümper and Ueda [2007] have described coincidence experiments and the random coincidences subtraction method in more details. Here, random triggers generated by an external pulse generator with 25 [Hz] frequency is utilized. All electron-triggered, random, and true coincidences are depicted in Fig. 5.

2.2 Electron spectra

PEPICO measurements provide both the TOF of ions, revealing the mass per charge ratio of the ions, as well as the kinetic energy of the ejected electrons. This technique is commonly used to analyze the unimolecular dissociation. However, analyzing catalytic reactions often involves dealing with multiple products and leftover reactants, making it difficult to distinguish parent molecules from ionization fragments. In these cases, coincidence ion yield photoelectron spectra (CIY-PES) can be used to provide additional information. For atoms, photoelectron spectroscopy shows the binding energies of the electrons, whereas for molecules, it reveals vibrational and rotational excitations as well. Photoelectron spectroscopy is a technique that can provide valuable insights into the energies, abundances, and angular distributions of electrons. Moreover, it reveals key features of the original molecular orbitals from which the electrons were emitted. On the other hand, isomers of a molecule have distinct electronic structures due to differences in the relative positioning of substituent groups, such as methyl groups in xylene, which can alter electronic density and molecular symmetry. This makes photoelectron spectroscopy a useful tool not only for distinguishing between different molecules but also for identifying various isomers of a molecule. For example, the photoelectron spectra obtained for meta- and para-xylene by Koenig et al. [1974] using He(I) radiation revealed that the first ionic states of these isomers have distinct vertical ionization potentials that can be utilized for differentiation purposes. Likewise, Ying et al. [1993] reported that unique features observed in the photoelectron spectra of cis-, trans-, and iso-butene can serve as distinctive markers to differentiate between these isomers. Therefore, utilizing CIY-PES can be a valuable tool for differentiating between ions with identical mass/fragments.

3 Experimental Part

3.1 GPES

This investigation has been performed at the gas-phase coincidence spectroscopy endstation (GPES) of the FinEst-BeAMS beamline at the MAX IV Laboratory (Lund, Sweden). The FinEstBeAMS beamline is in the 1.5 [GeV] storage ring providing photon energy in the range of ultraviolet to soft X-ray (i.e., 4.5 to 1300 [eV]) as well as variable polarization of synchrotron radiation. Detailed information on the design and optical concept of the FinEstBeAMS beamline is given elsewhere Pärna et al. [2017], Chernenko et al. [2021]. The FinEstBeAMS beamline consists of two separate branch lines. The gas-phase coincidence spectroscopy endstation (GPES) and the photoluminescence endstation (PLES) are in the same branch, while the solid-state end station (SSES) is located in the other one. The PLES, and SSES are designed for luminescence spectroscopy of solids, and photoelectron and X-ray absorption spectroscopy of surfaces and interfaces, respectively Chernenko et al. [2021]. The GPES is developed for electron and ion spectroscopy as well as photoelectron-photoion coincidence spectroscopy of low-density matter. Kosser et al. (2020) describes the GPES in more details. Briefly, in this apparatus an electron spectrometer (SCIENTA R4000) is utilized besides a Wiley-Maclaren ion time of flight (TOF) mass spectrometer to detect simultaneously the electrons and ions produced throughout the ionization. The schematic of the GPES is presented in Fig. 1.

3.2 Reactor

A portable, flange-mounted catalytic packed-bed reactor (length 50 [mm], ID 4 [mm]) was interfaced directly with the GPES end-station, as shown in Fig. 6. In brief, 20 [mg] of a catalytic sample was packed in the middle of the reactor as a thin (2 [mm]) layer sandwiched between two inert zones that were packed with quartz particles of the same sieve fraction. The reactor was resistively heated, while the temperature was monitored by a K-type thermocouple positioned in the middle of the catalytic bed. Gaseous reactants were fed into the reactor through a calibrated leak valve, and the effluent was allowed to freely enter the analysis chamber.

3.3 Materials and reagents

A commercial MFI zeolite (ZSM-5-MFI-27) was purchased from Sud Chemie. To obtain the acidic form of the catalyst, the as-received material was ion-exchanged with NH_4NO_3 , extensively washed, and calcined in static air at 550 [$^{\circ}\text{C}$] for 10 hours. Then, the catalyst was pressed into pellets that were sieved to $250 < d_p < 400$ [μm] size fraction, which were subsequently packed into the reactor. Before the experiment, the catalyst was maintained in vacuum at 550 [$^{\circ}\text{C}$] for 30 minutes to desorb the residual water. The detailed procedure for the catalyst preparation and extensive standard characterization data can be found in Rojo-Gama et al. [2018]. Basic physico-chemical properties were determined to be as follows: Si/Al ratio of 15, BAS concentration of 0.87 [mmol/g], crystal size of 2-6 [μm], and BET surface area of 398 [m^2/g].

3.4 PEPICO

Operando PEPICO was used to monitor the composition of the effluent stream of DME conversion on a ZSM-5 catalyst at a temperature of 375 [°C]. Pure DME was fed into the reactor at a rate of 1 [sccm] via a precision leak valve opening directly into the packed bed. At this feed rate, the pressure in the analysis chamber remained at 5×10^{-7} [mbar].

Photon energy of 40 [eV] was applied for this experiment in which the electron analyzer operates at pass energy of 100 [eV] with the kinetic energy window centered at 28 [eV]. Therefore, electrons with binding energy approximately in the range of 7 – 17 [eV] were collected with around 628 [mev] energy resolution. The electron count rate and random frequency were kept at about 25 [Hz]. In total, almost 1.9×10^6 triggers were detected, in which roughly 21% of them were coincidence triggers. Coincidence-specific data handling was done with custom Igor Pro macros written by Kukk et al. [2007].

4 Results and discussion

4.1 TOF spectra

The calibrated TOF spectrum of true ions detected in coincidence with electrons in the binding energy range of ca. 7 to 17 [eV] is depicted in Fig. 2b, representing the effluent stream during the conversion of dimethyl ether (DME) on a ZSM-5 catalyst. Due to the negligible intensity observed for ions with mass per charge ratios greater than 120, they are excluded from the figure. The detected ions are generated mainly by single valence ionisation as the cross section for direct double photoionization is low (therefore, for the sake of abbreviation, instead of mass per charge ratio, only mass is going to be used). In order to calibrate the TOF spectrum to masses, the following formula is utilized $m/z = (TOF - T_0)^2/C^2$. The calibration parameters are calculated by considering peaks corresponding to masses 2 (H_2) and 91 (C_7H_7) as references, and are found to be $T_0 = 1715$ [ns] and $C = -11.59$ [ns $(e/u)^{1/2}$]. A broad range of ions, covering masses from 1 to 156, are detected in the effluent stream. Table 2 lists the masses detected in true coincidences and the possible corresponding molecular ions.

Using dipole (e,e+ion) spectroscopy, Feng et al. Feng et al. [2001] determined the photoion branching ratios of DME in the equivalent photon energy range of 8.5 to 80 [eV] by utilizing TOF-MS. They reported that at 40 [eV] photon energy, the branching ratios of ions with masses 46 and 45 were about 13.6 and 22.5%, respectively. However, in the current experiment, ions with these masses are not detected (as shown in Table 2). Thus, it can be concluded that DME is not present in the effluent and its complete conversion is attained under the specified conditions considered in this study.

In Fig. 2b, the peak with the highest intensity corresponds to mass 18 - an expected result, considering that water is a major product of DME conversion on zeolite catalysts Chang [1983]. The peak with the second highest intensity corresponds to the mass 28, which can be attributed to N_2^+ , CO^+ , and/or $C_2H_4^+$ cations. However, it is not possible to determine from the TOF spectrum alone whether all of these cations contribute to this peak or not. Moreover, the peaks for masses 16 and 15 exhibit noticeable intensities in the recorded spectrum. CH_3^+ cation is the only plausible candidate for the peak with mass 15, given that the effluent is expected to contain hydrocarbons, water, and residual oxygenates (DME and methanol). However, it is possible that both CH_4^+ and O^+ contribute to the peak observed at the mass 16. Based on the peaks observed at masses 18, 28, 32, and 44, it is possible that the O^+ cation detected in the experiment originates from the fragmentation of H_2O , CO , O_2 , CH_3OH , or CO_2 molecules, respectively. Nonetheless, the absence of a peak at mass 31 implies that CH_3OH is not present in the effluent stream, consistently with a complete conversion of oxygenates on MFI-27 at these conditions. For the peak at mass 44, both CO_2^+ , and $C_3H_8^+$ are the possible cations that we can not discriminate only by TOF spectrum. There is a group of small peaks at masses 39 – 42, possibly due to photofragmentation of propylene.

The TOF spectra display a pair of peaks at masses 91 and 92, which correspond to $C_7H_7^+$ and $C_7H_8^+$, respectively, and are the major fragments of toluene. Moreover, the pair of peaks observed at 105 and 106 represent $C_8H_9^+$ and $C_8H_{10}^+$ cations, respectively. $C_8H_9^+$, $C_8H_{10}^+$, and $C_7H_7^+$ are the main fragments of xylene. Although the TOF spectrum provides valuable information about the potential parent molecules in the effluent stream, toluene and xylene in this case, it is not possible to determine the specific origin of the $C_7H_7^+$ cation.

In general, conventional mass spectroscopy techniques, including TOF, have limitations when it comes to analyzing the complex mixtures or molecules with identical masses, such as isomers. Hence, alternative techniques like PEPICO are employed to overcome these limitations and provide more detailed information about the parent molecules. This is achieved by recording the kinetic energy of the detected electrons and extracting CIY-PES for each detected masses. These spectra can then be compared with the previously reported spectra of potential parent molecules to validate the identification achieved by mass spectrometry.

4.2 PEPICO

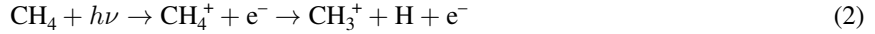
Fig. 2 shows an electron-energy-resolved PEPICO map of electronic states with binding energies between 8-17 [eV]. This map provides a two-dimensional view of the detected event intensities for all ion TOF - electron energy pairs. The horizontal axis corresponds to the electron hit position energies (which is calibrated to the electron binding energy in the top panel) and the vertical axis corresponds to the simultaneously detected ion flight times. This map provides an overview of the fragmentation patterns by associating specific electron binding energies with their corresponding positively charged fragments. False coincidences have been removed and slight smoothing is applied for better visualization. While the general trend can be seen in Fig. 2, a more detailed analysis should be conducted using the CIY-PES, which is given in the next section.

4.3 CIY photoelectron spectra

Fig. 2a illustrates the photoelectron spectrum (PES) of all detected electrons in coincidence with true ions. In this section, we aim to discriminate between the different species in the effluent stream by comparing the extracted CIY-PES with those previously reported for potential source compounds. To perform this comparative analysis, reference spectra are obtained via digitization using the WebPlotDigitizer online software Rohatgi [2022].

The TOF spectrum reveals two intense peaks at masses 15 and 16 (Fig. 2b). The peak at mass 15 corresponds only to the CH_3^+ cation, while that at mass 16 can be attributed to CH_4^+ and O^+ cations. The potential parent molecules that contain oxygen and can give rise to O^+ ion in this study are O_2 , CO, CO_2 , water, and DME. However, the mass spectra of these molecules, as reported by the NIST Chemistry WebBook Wallace [2018], would exhibit a considerably smaller peak at this mass. In our dataset, their molecular ions have lower intensity than the peak at mass 16. Therefore, it is assumed that CH_4^+ is the only cation contributing to the peak in question.

The ionization of a molecule can occur from different sites, including the bonding and antibonding orbitals. For CH_4 , the fragmentation channels are Chang et al. [2017]:



Therefore, aggregating the CIY-PESs collected with PEPICO for CH_3^+ and CH_4^+ can result in a spectrum that is more representative of CH_4 PES. Fig. 3a shows a comparison between the CIY-PES for masses 15 and 16, and their sum with the reference PES of CH_4 . The CIY-PES of mass 16 only covers a portion of the reference spectrum, while the CIY-PES of mass 15 covers the remaining section. The aggregation of these two spectra results in a spectrum that closely resembles the reference spectrum of CH_4 as reported by Kimura [1981], as expected from the aforementioned ionization channels.

Mass 18 exhibits the most prominent peak in the TOF spectrum, with water being the most likely species of origin, as stated previously. To verify this, the extracted CIY-PES for mass 18 is compared with the He(I) photoelectron spectrum of water in Fig. 3b Kimura [1981]. Despite the differences in the photon energies and the resolution, this figure demonstrates a favorable agreement between the measured and the reference spectra.

Based on the nature of the experiment, the most likely cations with mass 28 are C_2H_4^+ (a product of the reaction), CO^+ (a background spectator in the chamber), and N_2^+ (an air leak). Comparison of the corresponding CIY-PES for mass 28 with the reference He(I) photoelectron spectra of N_2 , CO, and C_2H_2 Kimura [1981] (see Fig. 7) reveals that N_2 and CO are present in the effluent stream. However, the reference spectrum for C_2H_4 displays a broad peak at binding energy of 14.66 [eV] which is not captured by the CIY-PES for mass 28. According to previous studies Wallace [2018], Stockbauer and Inghram [1975], in addition to the molecular ion C_2H_4^+ , pure C_2H_4 also fragments into C_2H_3^+ and C_2H_2^+ with masses 27 and 26, respectively. The combined CIY-PES for masses 26, 27, and 28, indeed, demonstrate a better agreement with the reference photoelectron spectrum of pure C_2H_4 , as presented in Fig. 3c.

The detection of N_2 indicates the presence of air leakage into the chamber, which is also confirmed by the observation of O_2 with a distinct peak at mass 32 in the TOF spectrum (Fig. 2b) and the corresponding comparison of CIY-PES with the reference photoelectron spectrum for O_2 Kimura [1981] (see Fig. 8).

Ions with masses of 41 and 42 are also detected with TOF mass spectrometer, albeit with low intensity. These ions could correspond to propylene (C_3H_6), which is an expected product of DME conversion, and ketene ($\text{C}_2\text{H}_2\text{O}$), which is a highly reactive intermediate of the reaction. Due to insufficient spectral resolution and low signal to noise ratio, it is not possible to delineate them from the PES. However, it can be inferred with confidence that the signal corresponds to propylene, since ketene is so reactive that it is not expected to survive the transport through the second inert zone in the reactor. The comparison between extracted CIY-PES for mass 42 and reference spectra for C_3H_6 and ketene is depicted in Fig. 3d. Ions with m/z of 44 likely originates from CO_2 and propane C_3H_8 , the former being present in the chamber

background and the latter being an expected minor product of DME conversion via hydrogen transfer reactions between propylene and methanol (see Fig. 9).

Ions with mass 56 are detected, which can be assigned to butene - another expected product of the reaction formed by methylation of propylene. However, the amount of butene produced was low and resulted in low signal-to-noise CIY-PES.

According to Cesarini et al. Cesarini et al. [2022], various isomers of C_5H_8 can undergo additional cyclization/dehydrogenation and methylation reactions, resulting in the formation of cyclopentadiene (C_5H_6 ; $m/z = 66$) and methyl cyclopentadiene (C_6H_8 ; $m/z = 80$), respectively. Furthermore, they have identified fulvene (C_6H_6 ; $m/z = 78$) formed through the dehydrogenation of methyl cyclopentadienes (C_6H_8). Fulvene is a precursor for the production of benzene, the first aromatic ring compound. Direct methylation of fulvene, as well as dehydrogenation-methylation of C_6H_8 , leads to the production of methyl fulvene (C_7H_8 ; $m/z = 92$), which is the primary precursor to toluene. This process can continue to generate other alkylated benzenes, including various isomers of xylene and trimethylbenzene. In the current experiment, masses 78 and 92 are detected, while 66 and 80 are not observed (Fig. 2b). To determine the identities of the detected peaks, a comparison between the CIY-PES obtained for masses 78 and 92, besides the relevant reference spectra are presented in Figs. 3e and 3f, respectively Kimura [1981], Cesarini et al. [2022]. The results indicate that benzene and toluene are the parent molecules associated with the detected peaks. However, it was not possible to detect intermediates such as fulvene and methyl fulvene in our experiments. We hypothesize that this limitation could be attributed to the experimental configuration of the reactor used in this study, i.e. the second inert zone of the packed bed.

In the present study, two peaks at masses 105 ($C_8H_9^+$) and 106 ($C_8H_{10}^+$) are observed in the TOF spectrum as shown in Fig. 2b. Considering the reaction mechanism, it is inferred that xylene (C_8H_{10}) is the appropriate parent molecule associated with these peaks. The CIY-PES for these ions by themselves do not fully coincide with the reference spectra of xylenes Koenig et al. [1974], Salaneck [1981] (see Fig. 10). This is because, in reference spectra, electrons from all ionization channels are considered, whereas, in CIY-PES, only electrons produced in specific ionization channels are taken into account. Fig. 3g displays the aggregation of CIY-PES for mass per charge ratios of 106, 105, and 91 that more closely matches the reference spectra. This suggests that the effluent stream contains a combination of different isomers of C_8H_{10} , with m-xylene appearing to be the most abundant isomer. Xylene isomerism offers a convenient benchmark problem for quantitative isomer discrimination, described in detail in section 4.4, which is a novel aspect in PEPICO analysis introduced in our work.

In addition to the various isomers of xylene, isomers of trimethylbenzene can be generated through direct methylation or dehydrogenation-methylation of lighter hydrocarbons Cesarini et al. [2022]. Despite the detection of only a negligible number of cations with mass 120 in the TOF spectrum (Fig. 2b), the comparison of the extracted CIY-PES with reference spectra (Fig. 3h) indicates the presence of a mixture of different isomers of trimethylbenzenes in our experiment Longetti et al. [2020].

4.4 Isomer quantification

Quantitative discrimination of isomers from PEPICO data would provide a valuable tool for analyzing complex reaction pathways in catalytic reactions of hydrocarbons. The measured reference spectra for different isomers of xylene are depicted in Fig. 3g along with the CIY-PES for combination of masses 106, 105, and 91 from the reactor effluent stream. The major differences between these spectra lies in their first and third bands in the 8 – 10 and 13 – 14 [eV] regions of binding energy, respectively. The ionization channel of $C_8H_{10} + h\nu \rightarrow C_8H_{10}^+ + e^-$ is correlated to the electrons with binding energy of 8 – 10 [eV]. Moreover, for the reference spectra, electrons coming from the background (H_2O , N_2 , and O_2) do not overlap with xylene electrons coming from ionization channel of $C_8H_{10}^+$. Therefore, we are going to focus on the first band to quantitatively distinguish the ratio of different isomers of xylene in the effluent.

The comparison between CIY-PES for mass 106 with reference spectra of xylene isomers is given in Fig. 4d. Considering the overall shape of the spectra, not only the coincidence ion yield PES does not have two separate peaks, similar to p-xylene, but also its FWHM is almost equal to meta xylene. Therefore, m-xylene is the dominant isomer among the products. But what is the exact branching ratio?

In order to quantitatively determine the ratio of isomers, firstly, each spectrum has been deconvoluted using a collection of asymmetrically distorted Voigt profiles, which each of them is a convolution of a Gaussian $G(x)$ and a Lorentzian $L(x)$:

$$V(x) = \int_{-\infty}^{\infty} G(\xi)L(x - \xi)d\xi \quad (3)$$

For reference PES of m- and p-xylene, aggregation of three Voigt profiles is required to adequately describe the collected data (Fig. 4a, b, respectively).

$$PES_{m-xylene} = \omega_1^m \cdot V_1^m + \omega_2^m \cdot V_2^m + \omega_3^m \cdot V_3^m \quad (4)$$

$$PES_{p-xylene} = \omega_1^p \cdot V_1^p + \omega_2^p \cdot V_2^p + \omega_3^p \cdot V_3^p \quad (5)$$

To predict the isomer ratio for CIY-PES of mass 106 in the effluent stream, these two groups of peaks were mixed in a specific ratio, while the peak shapes, center distances, and intensity ratios within each group were fixed according to their values estimated from pure reference compounds (i.e. m- and p-xylene). First, the method was benchmarked against two control mixtures of m- and p-xylanes with known compositions, 50:50 and 75:25, returning estimates of 56:44 and 77:23, respectively. This outcome demonstrates that, although promising, the isomer quantification analysis requires PEPICO data with higher signal to noise ratio and more systematic collection of calibration datasets.

Next, we applied the same routine to analyze the reactor effluent. Fig. 4c demonstrates the quality of the resulting model fit. Based on this method, and considering the area of peaks, almost 85% of the electrons detected in coincidence with $C_8H_{10}^+$ cation are coming from m-xylene and the remaining 15% are related to p-xylene. This result agrees well with the selectivities reported in the literature for unmodified ZSM-5 Zhang et al. [2015].

5 Conclusion

Operando Photoelectron–Photoion Coincidence (PEPICO) mass-spectrometry is emerging as a valuable analytical tool for investigations of reaction mechanisms and kinetics in heterogeneous catalysis. Currently, the scope of the technique and its adoption in the catalysis research community are constrained by the limited availability of dedicated facilities around the globe. We have established a new location - the FinEstBeAMS beamline at MAX-IV Laboratory - at which PEPICO and, in fact, other coincidence-based methods can be used to analyze the effluent of a catalytic reactor. This capability was demonstrated using Dimethyl Ether conversion on a prototypical ZSM-5 catalyst (at 375 [$^{\circ}C$] and 5×10^{-7} [mbar] total pressure) as a benchmark reaction, which agreed with the product distribution expected from the literature. Due to the specific configuration of the reactor packing in our proof-of-principle study, we have not observed either ketene or methyl radical, both highly-reactive intermediates that were recently revealed by *operando* PEPICO, which will be addressed in future work. Finally, we have quantitatively determined the ratio of xylene isomers in the product stream by deconvoluting their coincidence photoelectron spectra, opening up a new avenue for quantitative isomer-selective PEPICO analysis in kinetic studies of heterogeneously catalyzed reactions.

6 Acknowledgements

This research was funded by the Research Council of Norway (#272266, TAPXPS project) and the Research Council of Finland (#341288, IntriCAT project). We acknowledge MAX IV Laboratory for time on FinEstBeAMS Beamline under Proposals 20190444 and 20180449. Research conducted at MAX IV, a Swedish national user facility, is supported by the Swedish Research council under contract 2018-07152, the Swedish Governmental Agency for Innovation Systems under contract 2018-04969, and Formas under contract 2019-02496. We express our gratitude to Dr. Antti Kivimäki and Dr. Kirill Chernenko at the FinEstBeAMS beamline, MAX IV Laboratory for their assistance during the experiments.

References

Unni Olsbye, Stian Svelle, Morten Bjørgen, Pablo Beato, Ton VW Janssens, Finn Joensen, Silvia Bordiga, and Karl Petter Lillerud. Conversion of methanol to hydrocarbons: how zeolite cavity and pore size controls product selectivity. *Angewandte Chemie International Edition*, 51(24):5810–5831, 2012.

Patrick Hemberger, Jeroen A van Bokhoven, Javier Pérez-Ramírez, and Andras Bodi. New analytical tools for advanced mechanistic studies in catalysis: photoionization and photoelectron photoion coincidence spectroscopy. *Catalysis Science & Technology*, 10(7):1975–1990, 2020.

Evgeniy A Redekop, Andrea Lazzarini, Silvia Bordiga, and Unni Olsbye. A temporal analysis of products (tap) study of c2-c4 alkene reactions with a well-defined pool of methylating species on zsm-22 zeolite. *Journal of catalysis*, 385:300–312, 2020.

Kuno Kooser, Antti Kivimäki, Paavo Turunen, Rainer Pärna, Liis Reisberg, Marco Kirm, Mika Valden, Marko Huttula, and Edwin Kukk. Gas-phase endstation of electron, ion and coincidence spectroscopies for diluted samples at the finestbeams beamline of the max iv 1.5 gev storage ring. *Journal of Synchrotron Radiation*, 27(4):1080–1091, 2020.

Tiberiu Arion and Uwe Hergenhahn. Coincidence spectroscopy: Past, present and perspectives. *Journal of Electron Spectroscopy and Related Phenomena*, 200:222–231, 2015.

Wu Wen, Shengsheng Yu, Chaoqun Zhou, Hao Ma, Zhongyue Zhou, Chuangchuang Cao, Jiuzhong Yang, Minggao Xu, Fei Qi, Guobin Zhang, et al. Formation and fate of formaldehyde in methanol-to-hydrocarbon reaction: In situ synchrotron radiation photoionization mass spectrometry study. *Angewandte Chemie International Edition*, 59(12):4873–4878, 2020.

Alessia Cesarini, Sharon Mitchell, Guido Zichittella, Mikhail Agrachev, Stefan P Schmid, Gunnar Jeschke, Zeyou Pan, Andras Bodi, Patrick Hemberger, and Javier Pérez-Ramírez. Elucidation of radical-and oxygenate-driven paths in zeolite-catalysed conversion of methanol and methyl chloride to hydrocarbons. *Nature Catalysis*, pages 1–10, 2022.

Andras Bodi, Patrick Hemberger, David L Osborn, and Bálint Sztáray. Mass-resolved isomer-selective chemical analysis with imaging photoelectron photoion coincidence spectroscopy. *The Journal of Physical Chemistry Letters*, 4(17):2948–2952, 2013.

WC Wiley and Ii H McLaren. Time-of-flight mass spectrometer with improved resolution. *Review of scientific instruments*, 26(12):1150–1157, 1955.

G Prümper and K Ueda. Electron–ion–ion coincidence experiments for photofragmentation of polyatomic molecules using pulsed electric fields: Treatment of random coincidences. *Nuclear Instruments and Methods in Physics Research Section A: Accelerators, Spectrometers, Detectors and Associated Equipment*, 574(2):350–362, 2007.

T Koenig, M Tuttle, and RA Wielesek. The he (i) photoelectron spectra of xylenes and metacyclophanes. a reassignment of the lowest ionic state of [2.2] metacyclophane. *Tetrahedron Letters*, 15(29):2537–2540, 1974.

JF Ying, H Zhu, CP Mathers, BN Gover, MP Banjavčić, Y Zheng, CE Brion, and KT Leung. Electron-momentum-specific valence-shell electronic structures of cis-, trans-, and iso-butene by symmetric noncoplanar (e, 2 e) spectroscopy. *The Journal of chemical physics*, 98(6):4512–4519, 1993.

Rainer Pärna, Rami Sankari, Edwin Kukk, E Nõmmiste, Mika Valden, Marko Lastusaari, Kuno Kooser, Kalevi Kokko, Mika Hirsimäki, Samuli Urpelainen, et al. Finestbeams—a wide-range finnish-estonian beamline for materials science at the 1.5 gev storage ring at the max iv laboratory. *Nuclear Instruments and Methods in Physics Research Section A: Accelerators, Spectrometers, Detectors and Associated Equipment*, 859:83–89, 2017.

Kirill Chernenko, Antti Kivimäki, Rainer Pärna, Weimin Wang, Rami Sankari, Mats Leandersson, Hamed Tarawneh, Vladimir Pankratov, Mati Kook, Edwin Kukk, et al. Performance and characterization of the finestbeams beamline at the max iv laboratory. *Journal of Synchrotron Radiation*, 28(5), 2021.

Daniel Rojo-Gama, Lukasz Mentel, Georgios N Kalantzopoulos, Dimitrios K Pappas, Iurii Dovgaluk, Unni Olsbye, Karl Petter Lillerud, Pablo Beato, Lars F Lundsgaard, David S Wragg, et al. Deactivation of zeolite catalyst h-zsm-5 during conversion of methanol to gasoline: operando time-and space-resolved x-ray diffraction. *The Journal of Physical Chemistry Letters*, 9(6):1324–1328, 2018.

E Kukk, R Sankari, M Huttula, A Sankari, H Aksela, and S Aksela. New electron-ion coincidence setup: Fragmentation of acetonitrile following n 1s core excitation. *Journal of electron spectroscopy and related phenomena*, 155(1-3):141–147, 2007.

Renfei Feng, Glyn Cooper, and CE Brion. Ionic photofragmentation and photoionization of dimethyl ether in the vuv and soft x-ray regions (8.5–80 ev)—absolute oscillator strengths for molecular and dissociative photoionization. *Chemical Physics*, 270(2):319–332, 2001.

Clarence D. Chang. Hydrocarbons from methanol. *Catalysis Reviews*, 25(1):1–118, 1983. doi:10.1080/01614948308078874. URL <https://doi.org/10.1080/01614948308078874>.

Ankit Rohatgi. Webplotdigitizer: Version 4.6, 2022. URL <https://automeris.io/WebPlotDigitizer>.

William E Wallace. Mass spectra. *NIST chemistry webbook, NIST standard reference database*, (69):20899, 2018.

Yih-Chung Chang, Bo Xiong, David H Bross, Branko Ruscic, and CY Ng. A vacuum ultraviolet laser pulsed field ionization-photoion study of methane (ch 4): determination of the appearance energy of methyllium from methane with unprecedented precision and the resulting impact on the bond dissociation energies of ch 4 and ch 4+. *Physical Chemistry Chemical Physics*, 19(14):9592–9605, 2017.

Katsumi Kimura. *Handbook of HeI photoelectron spectra of fundamental organic molecules*. Halsted Press, 1981.

Roger Stockbauer and Mark G Inghram. Threshold photoelectron–photoion coincidence mass spectrometric study of ethylene and ethylene-d 4. *The Journal of Chemical Physics*, 62(12):4862–4870, 1975.

W. R. Salaneck. *Intermolecular Relaxation Effects in the Ultraviolet Photoelectron Spectroscopy of Molecular Solids*, chapter 11, pages 121–149. ACS Publications, 1981. doi:10.1021/bk-1981-0162.ch011. URL <https://pubs.acs.org/doi/abs/10.1021/bk-1981-0162.ch011>.

L Longetti, M Randulová, J Ojeda, L Mewes, L Miseikis, J Grilj, A Sanchez-Gonzalez, T Witting, T Siegel, Z Diveki, et al. Photoemission from non-polar aromatic molecules in the gas and liquid phase. *Physical Chemistry Chemical Physics*, 22(7):3965–3974, 2020.

Jingui Zhang, Weizhong Qian, Chuiyan Kong, and Fei Wei. Increasing para-xylene selectivity in making aromatics from methanol with a surface-modified Zn/P/ZSM-5 catalyst. *ACS Catalysis*, 5(5):2982–2988, 2015.

Zhongyue Zhou, Xuewei Du, Jiuzhong Yang, Yizun Wang, Chaoyang Li, Shen Wei, Liangliang Du, Yuyang Li, Fei Qi, and Qiuping Wang. The vacuum ultraviolet beamline/endstations at NSRL dedicated to combustion research. *Journal of synchrotron radiation*, 23(4):1035–1045, 2016.

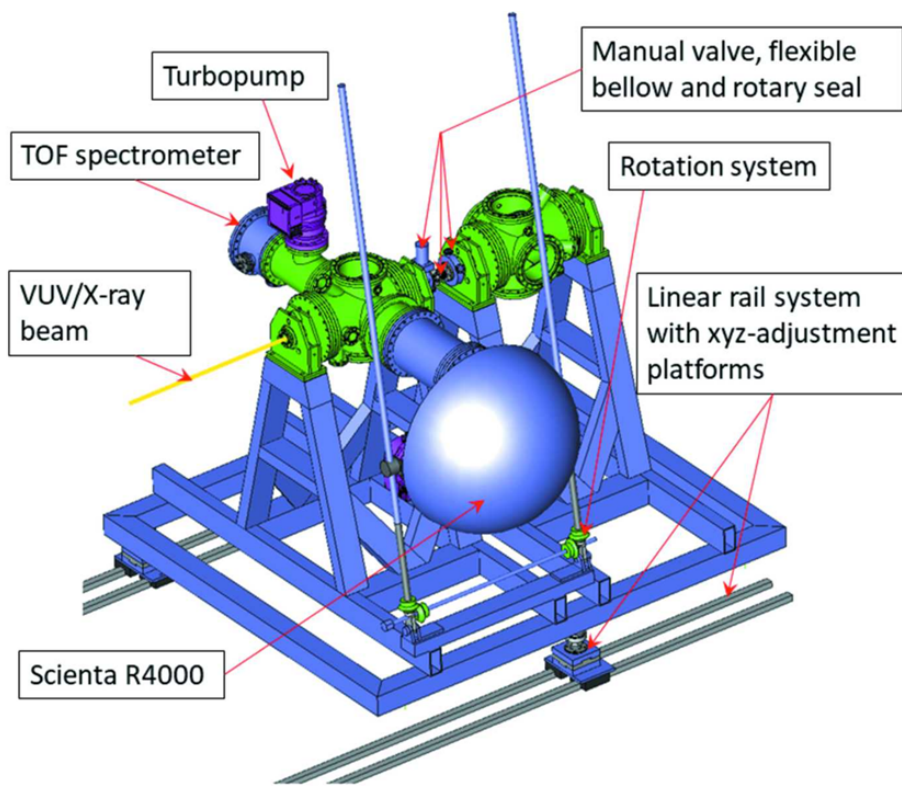


Figure 1: Gas-phase endstation at the FinEstBeAMS beamline of the MAX IV Laboratory. Reproduced with permission from reference Kooser et al. [2020].

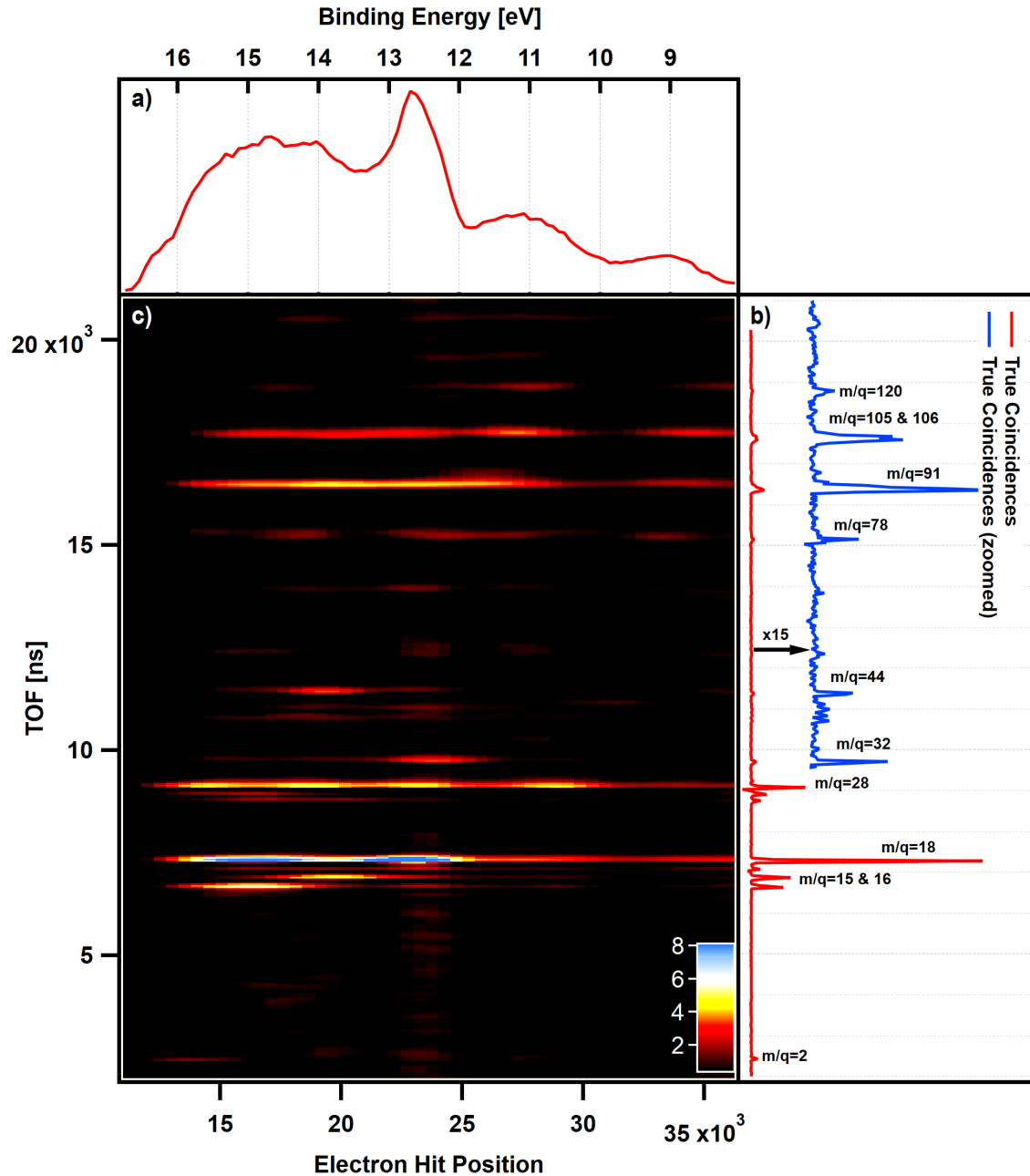


Figure 2: PEPICO map of the effluent stream of DME conversion over ZSM5 zeolite at 375 [°C] ionized using light with 40 [eV] energy. Top panel: integrated binding energy spectrum. Right panel: integrated ion TOF spectrum with false coincidences subtracted. For higher TOF, the spectrum intensity is multiplied by 10, to make it more clear. The corresponding mass per charge ratios are mentioned for groups of TOF peaks.

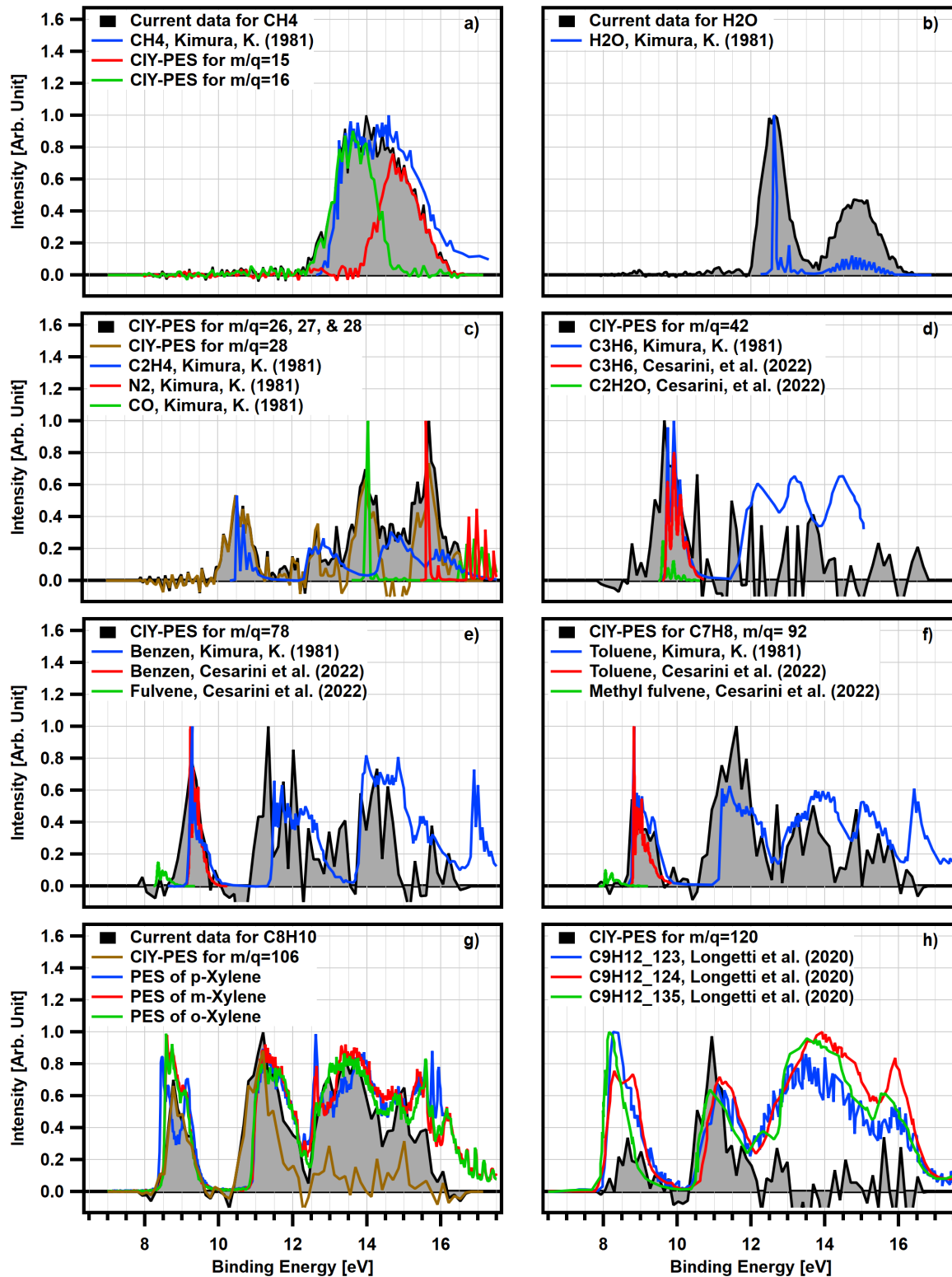


Figure 3: The comparison of extracted coincidence ion yield photoelectron spectra (CIY-PES) at 40 [eV] photon energy with reference spectra for most intense detected cations Kimura [1981], Cesarini et al. [2022], Koenig et al. [1974], Longetti et al. [2020].

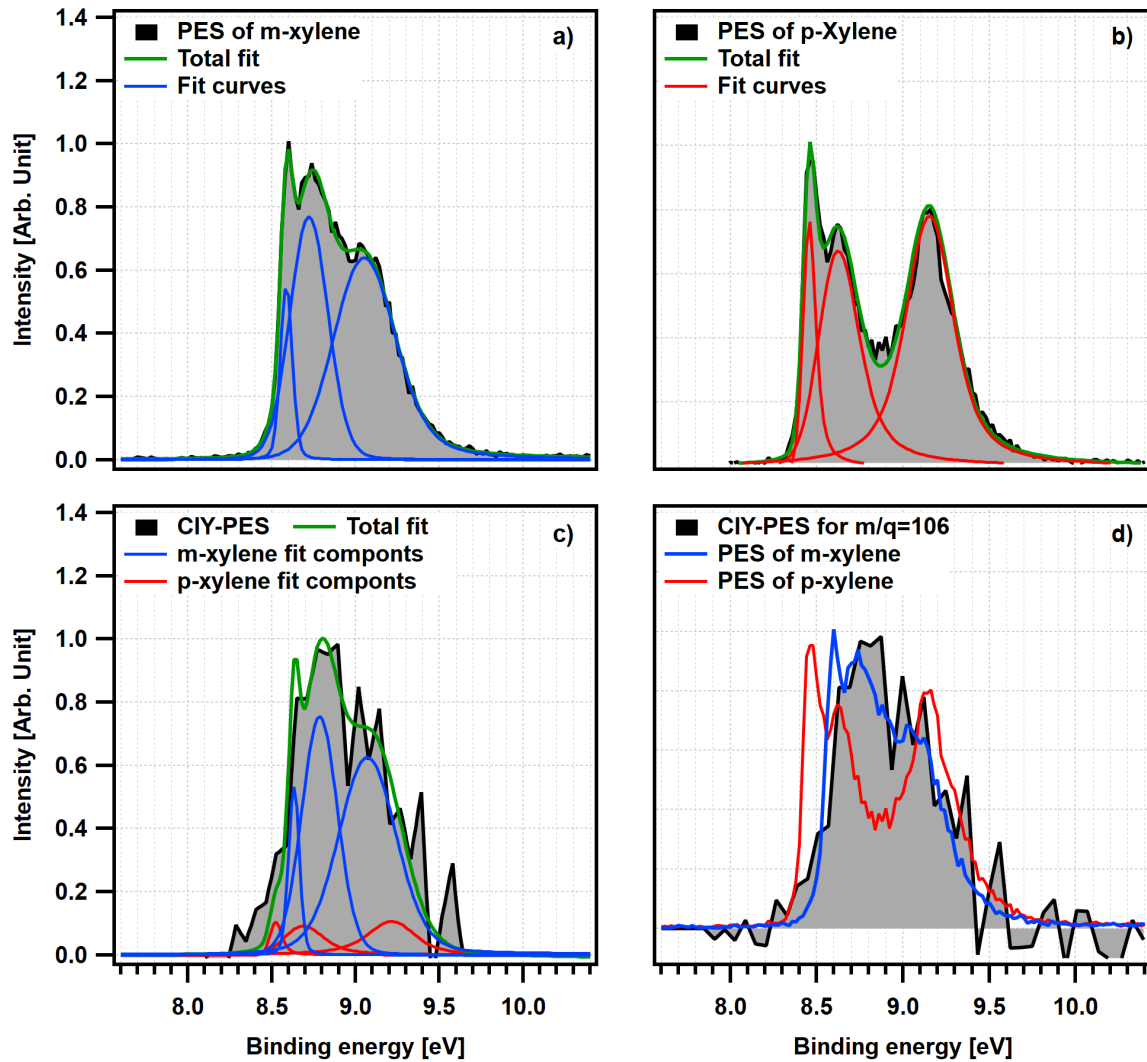


Figure 4: CIY-PES for mass 106 with peak deconvolution, d) CIY-PES for mass 106 with bin size = 200 and 0.06 eV shifted

Table 1: Catalytic experiments at FinEstBeANS in the global context

Facility	Beamline	Pressure range, [mbar]	Energy range, [eV]	Analyzer	Detector	Techniques
SLS ^a	VUV	$10^{-8} - 10^3$	3 – 150	e-TOF	position-sensitive DLD	PIMS iPEPICO
				ion-TOF	position-sensitive DLD	i ² PEPICO
NSRL	BL03U	$10^{-8} - 10^3$	5 – 21	ion-TOF	MCP + cone-shaped stainless steel anode Zhou et al. [2016]	PIMS
SOLEIL	DESIRS (SAPHIRS end station)	$10^{-8} - \text{a few mbars}$	5 – 40	e-TOF	position-sensitive detector	i ² PEPICO
				ion-TOF	position-sensitive detector	
MAX IV	FinEstBeAMS (GPES)	$10^{-8} - 10^{-6}$ ^b	4.5 – 1300	HSA	resistive anode	XPS PIMS(<1s)
				ion-TOF	position-sensitive DLD	PEPICO PIPICO

^a SLS shutdown in 2023 will limit global PEPICO capacity for a few years.

^b Differentially-pumped Molecular Beam Extraction (MBE) for experiments up to 10^3 [mbar] is under design/construction at the University of Oulu.

Table 2: Detailed breakdown of ionisation fragments at 40 [eV] photon energy (in coincidence with 7 to 17 [eV] binding energy), corresponding to the TOF spectrum of true coincidences

Mass [amu]	Chemical formula	Mass [amu]	Chemical formula
1	H ⁺	39-42	C ₃ H _n ⁺ ($n = 3 - 6$)
2	H ₂ ⁺	44	CO ₂ ⁺
14	N ⁺	50-52	C ₄ H _n ⁺ ($n = 2 - 4$)
15-16	CH _n ⁺ ($n = 3 - 4$)	65	C ₅ H ₅ ⁺
17	OH ⁺	77-78	C ₆ H _n ⁺ ($n = 5 - 6$)
18	H ₂ O ⁺	91-92	C ₇ H _n ⁺ ($n = 7 - 8$)
26-27	C ₂ H _n ⁺ ($n = 2 - 3$)	105-106	C ₈ H _n ⁺ ($n = 9 - 10$)
28	C ₂ H ₄ ⁺ , N ₂ ⁺ , CO ⁺	120	C ₉ H ₁₂ ⁺
29-30	C ₂ H _n ⁺ ($n = 5 - 6$)	128	C ₁₀ H ₈ ⁺
32	O ₂ ⁺	141-142	C ₁₁ H _n ⁺ ($n = 9 - 10$)
37	C ₃ H ⁺	156	C ₁₂ H ₁₂ ⁺

A Supplementary information

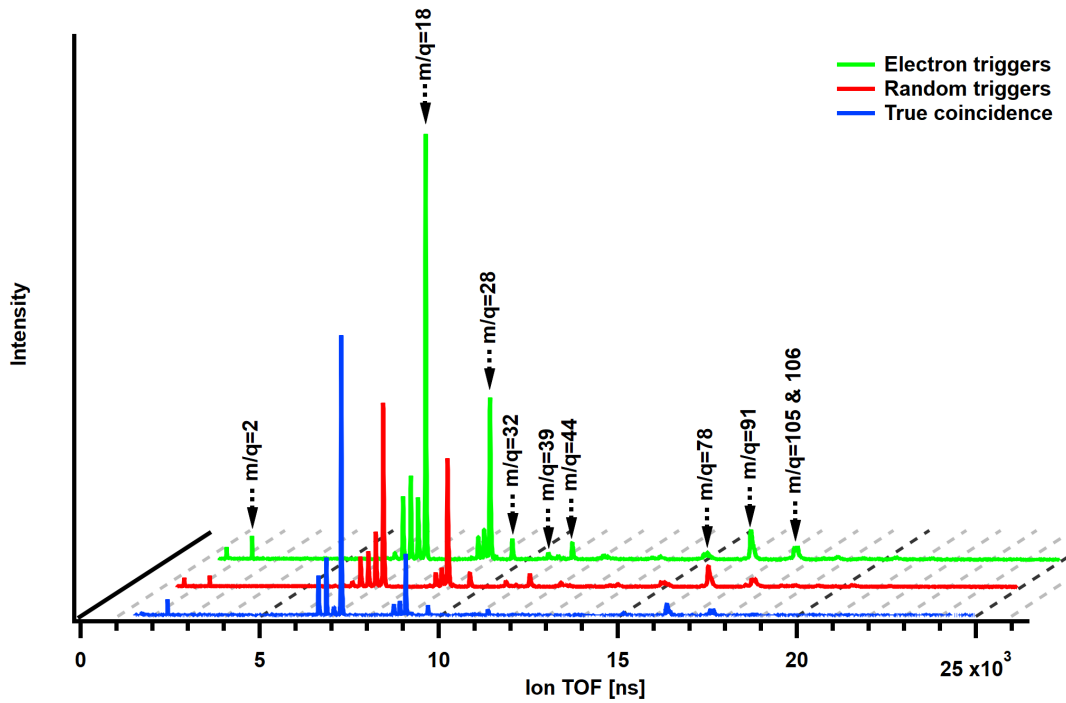


Figure 5: The TOF spectra of ions for random triggers, electron triggers, and true coincidences recorded with photon energy of 40 [eV].

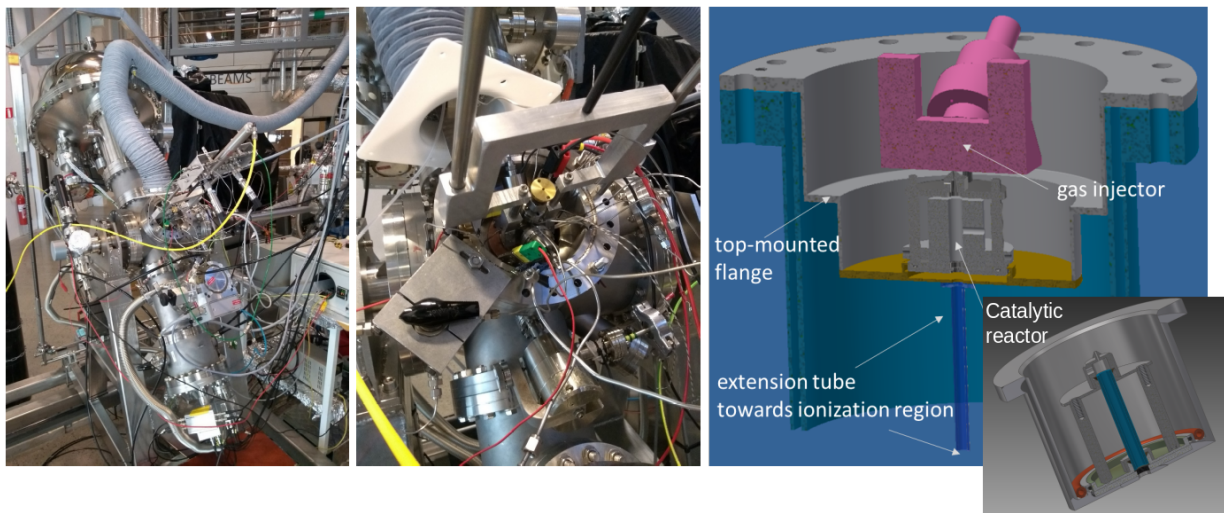


Figure 6: The real time pictures of the GPES end-station with the schematic of the utilized reactor.

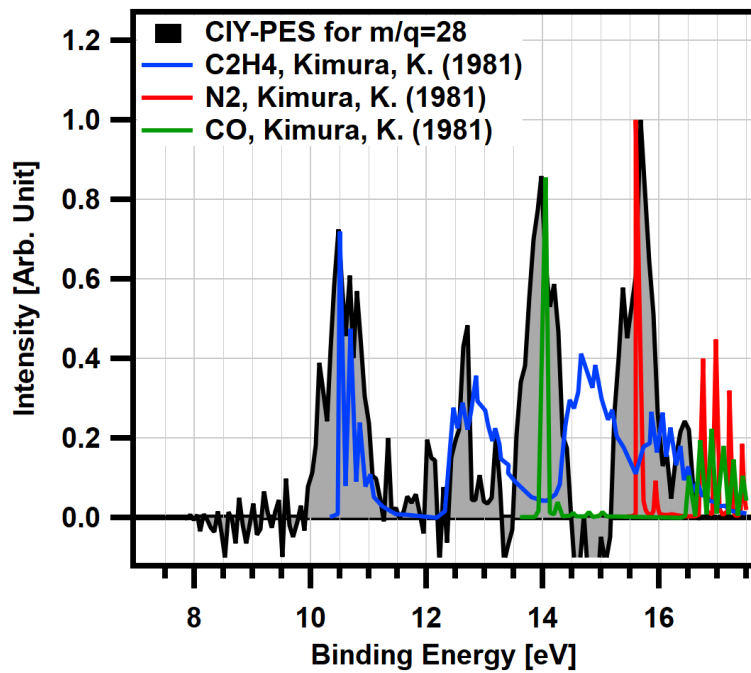


Figure 7: The comparison of extracted coincidence ion yield PES at 40 [eV] photon energy with reference spectra for ions with $m/q = 28$ Kimura [1981].

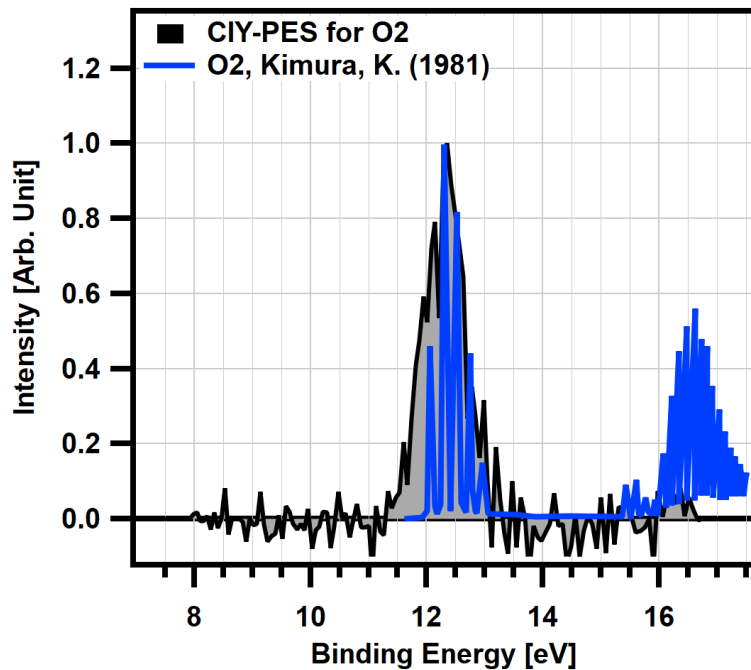


Figure 8: The comparison of extracted coincidence ion yield PES at 40 [eV] photon energy with reference spectra for ions with $m/q = 32$ Kimura [1981].

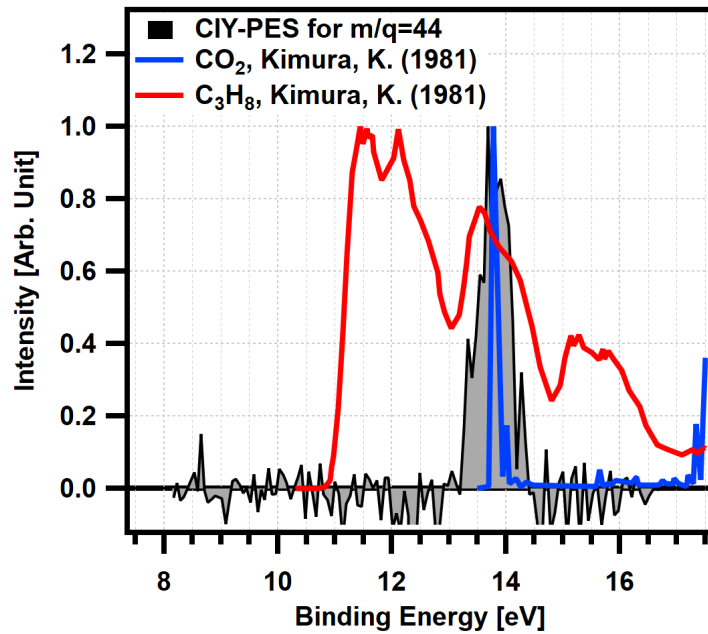


Figure 9: The comparison of extracted coincidence ion yield PES at 40 [eV] photon energy with reference spectra for ions with $m/q = 44$ Kimura [1981].

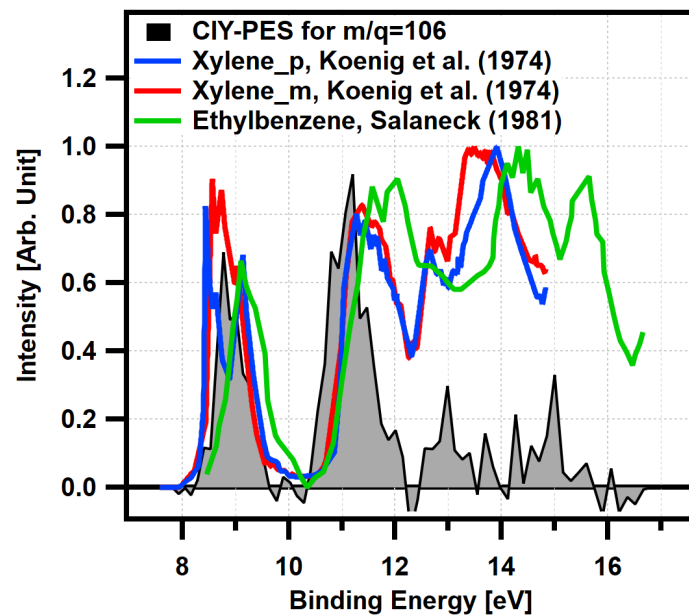


Figure 10: The comparison of extracted coincidence ion yield PES at 40 [eV] photon energy with reference spectra for ions with $m/q = 106$ Koenig et al. [1974], Salaneck [1981].